Magnetic Field Intensity Measurements in CF/LANR/Manelis Experiments

Mitchell Swartz, ScD, MD, EE AC1ER Nanortech, Inc Feb. 13, 2020 draft

1. Experimental – Dual Frequency insertion through Magnetic Hoops

Helmholtz Coils (hoops) , used along one to three perpendicular axes
Maxwell coils (Three coils) Helmholtz Bobbins - The two coil bobbins will be 3D printed
Coil Driver voltage follower MCP602 dual op amp NPN BC337 emitter follower

2. Experimental – Helmholtz Coils

Helmholtz coils (hoops) are here used to generate an additional complex magnetic field intensity imposed on the active NANOR component or control. Normally they are used along one to three perpendicular axes, to either cancel the Earth's magnetic field or used to create a near uniform applied magnetic field intensity (Figure 1). They are on sale on Ebay (Figure 2).

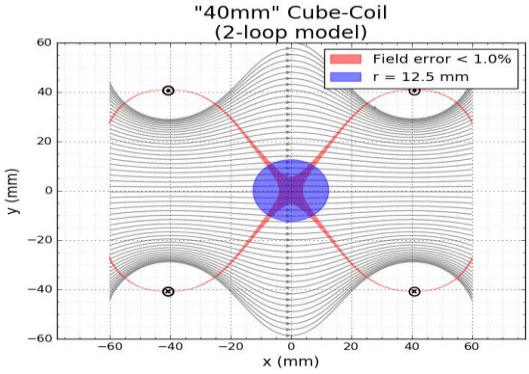

Figure 7 - **Helmholtz coils** - left: two coils and the intensity of their magnetic field outputs, each alone and superimposed; right: the 2D variations of the applied magnetic field intensity near the central axis showing near uniformity. after Google

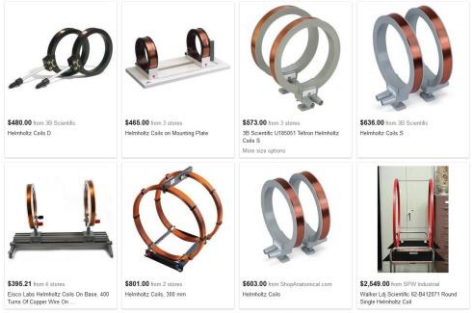

Figure 2 - Helmholtz coils on sale after Google

The Intensity of the Applied Magnetic field Generated by Two Helmholtz coils:

To setup a Helmholtz coil two similar coils with radius R are placed in the same distance R. When the coils are so connected that the current through the coils flows in the same direction, the Helmholtz coils produce a region with a nearly uniform magnetic field.

The applied magnetic field intensity is derived by superposition and the Biot-Savart law. The magnetic field at center of the coils with N wire windings is proportional to current through coils:

$$B = [\mu_0 \cdot 8 \cdot I \cdot N] / [\text{sqrt}(125) * R]$$

I = coil current, μ_0 = vacuum permeability, N = windings,
R = radius and distance of coils, $\mu_0 = 4\pi \cdot 10^{-7}$

3. Experimental – Maxwell coils (Three coils)

To further improve the uniformity of the applied field, an additional coil was added by James Clerk Maxwell (1873), slightly larger and located midway between the two Helmholtz coils (Figure 9). He reported that this addition diminished the variance of the field on the axis to zero up to the sixth derivative of position. This third coil is called a 'Maxwell coil'. This arrangement removes variations in magnetic field, up to its 6th-order derivative with respect to position, near the center of a virtual sphere.

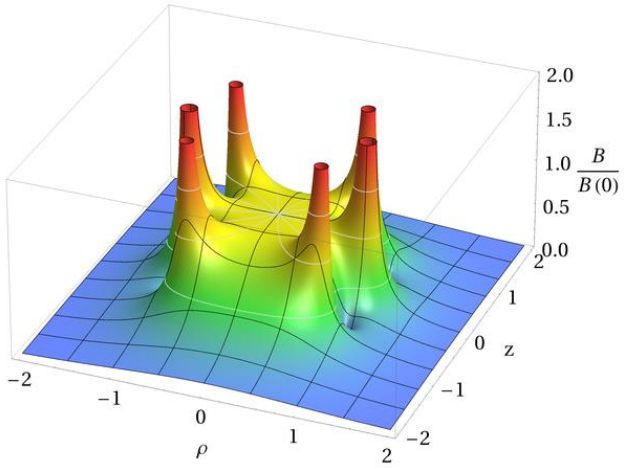

Figure 3 - Maxwell coils - left: three coils and the isointensity of their magnetic field outputs, superimposed; right: the 3D variations of the applied magnetic field intensity near the central axis showing very near uniformity. after Google

According to Maxwell's original 1873 design, a constant-field Maxwell coil set consists of three coils oriented on the surface of a virtual sphere. Each of the outer coils should be of radius sqrt(4/7)*R, and distance sqrt(3/7)*R, from the plane of the central coil of radius R. The number of ampere-turns of each of the smaller coils should equal exactly 49/64 of the middle coil.

Have been unable to 3D print so far the Maxwell variant for size reasons. Therefore, for our upcoming ESR experiments, the first system will use wound Hemholz coils, there are two. Each has 300 turns of 0.15 mm enameled copper wire, with an internal diameter of 12mm.
Background on electrostatics
https://www.didaktik.physik.uni-muenchen.de/elektronenbahnen/en/b-feld/B-Feld/Helmholtzspulenpaar.php

4. Experimental – Magnetic Sensors

To measure magnetic flux density, tried three sensors.

1-UGN3503U TO-92 Ratiometric Linear HALL-EFFECT – Useful at high fields

The off-label use of UGN3503U TO-92 Ratiometric Linear HALL-EFFECT ICs was useful for very high magnetic field intensities. They are used for switching, but here are quite useful because they are (reportedly) linear. Here are two results.

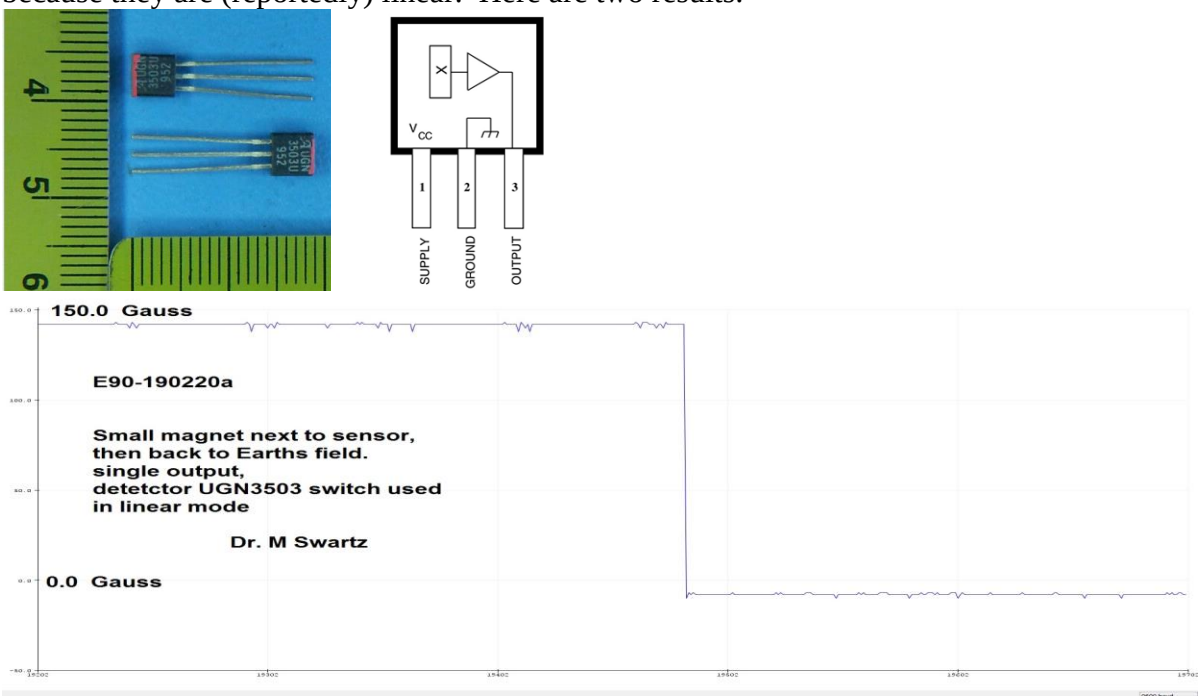

Figure 4- UGN3503U TO-92 Ratiometric Linear HALL-EFFECT

Figure 5 - UGN3503U TO-92 Ratiometric Linear HALL-EFFECT

Not only off label use, but it was difficult to find working code to run it. This worked for both the serial port and plotting.

```
/*  JET Energy GaussPlot 27/12/2011  Arduino
Showing Gauss measured by Miniature Radiometric Linear Hall Efect Sensor
connected to Analog channel 0.
*/
#define XRANGE  50
int x,gss;
void setup(){
  Serial.begin(9600);
}
void loop(){
  int aValue =analogRead(0);
  x = map(aValue, 0, 1024, 0, XRANGE);
  gss = map(aValue, 102, 922, -640, 640);
//  Serial.print("|");
//  for (int i=0;i<x;i++){
//    if(i==XRANGE/2-1)Serial.print("|");
//    else Serial.print("-");
// }
// Serial.print("O");
//  for (int i=x+1;i<XRANGE;i++){
//    if(i==XRANGE/2-1)Serial.print("|");
//   else Serial.print("-");
//  }
//  Serial.print("|");
  Serial.println(gss);
  //Serial.print "";

 // Serial.println("Gauss");
  delay(100);
```

6**. The HMC5883 L Magnetometer - Sensitive at low magnetic field intensities**

The HMC5883L was tried, and it was very sensitive and worked well.

Specs: I2C interface, 12-bit ADC, 160Hz max data rate, Range of -8 to +8 Gauss

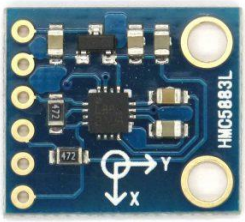

Figure 6

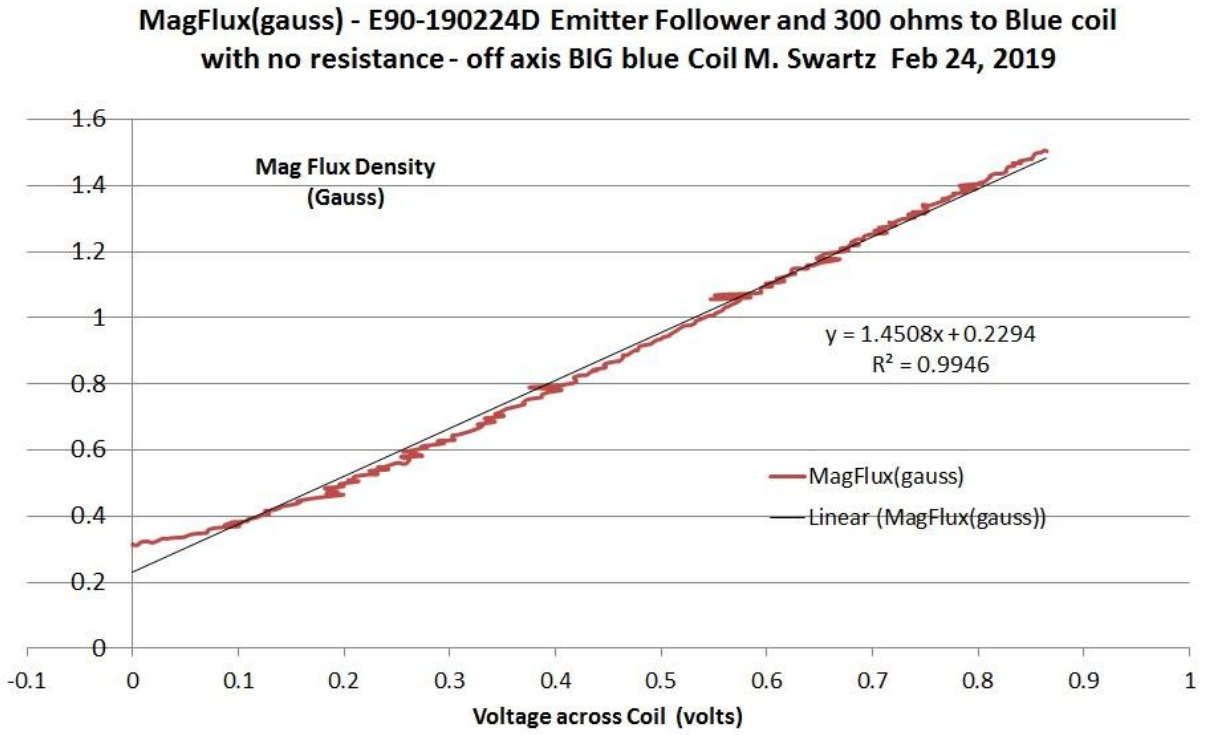

Figure 7 - HMC5883 L Magnetometer in Emitter follower setup, off axis.

7. BNO055 Hall sensor - DOA

This sensor, the Adafruit 9-DOF Absolute Orientation IMU Fusion Breakout - BNO055, MEMS accelerometer, magnetometer and gyroscope did not work well. It is unclear why, but – consistent with these findings -there is much criticism of this chip on the Internet. No further time was given.

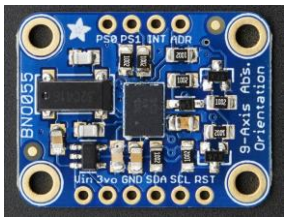

Magnetic Field Strength Vector (20Hz)

Interest was using three axis of magnetic field sensing in micro Tesla (uT). Additionally, specs reveal it uses I2C address 0x28 (default) or 0x29, Three axis orientation data based on a 360° sphere, Four point quaternion output, Three axis of 'rotation speed' in rad/s, Three axis of acceleration (gravity + linear motion) in m/s^2, Three axis of magnetic field sensing in micro Tesla (uT), Three axis of linear acceleration data (acceleration minus gravity) in m/s^2, Three axis of gravitational acceleration (minus any movement) in m/s^2, and Ambient temperature in degrees Celsius.

Figure 9-11 - With Programmable Source

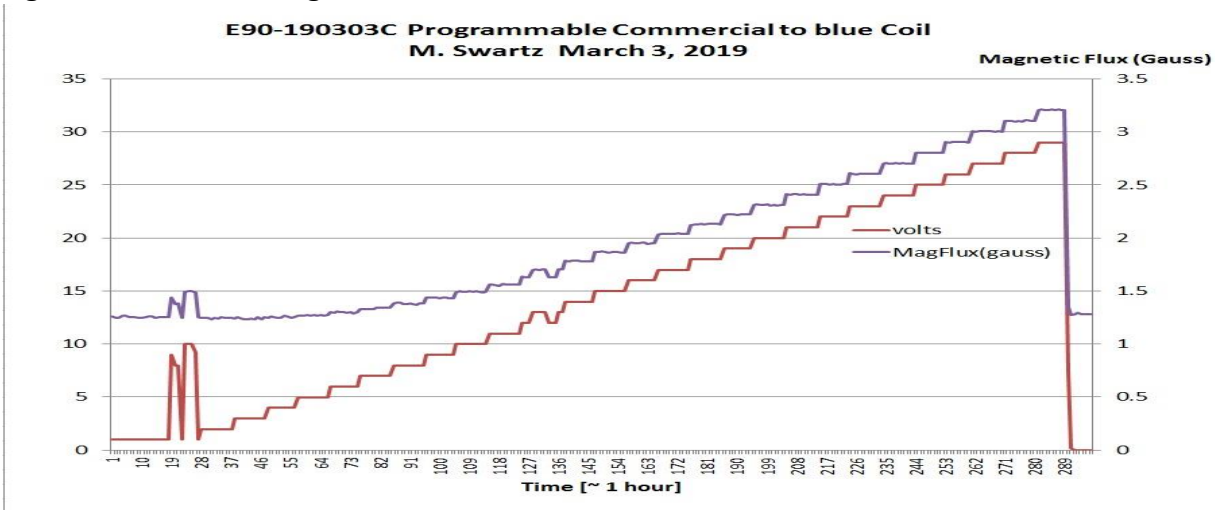

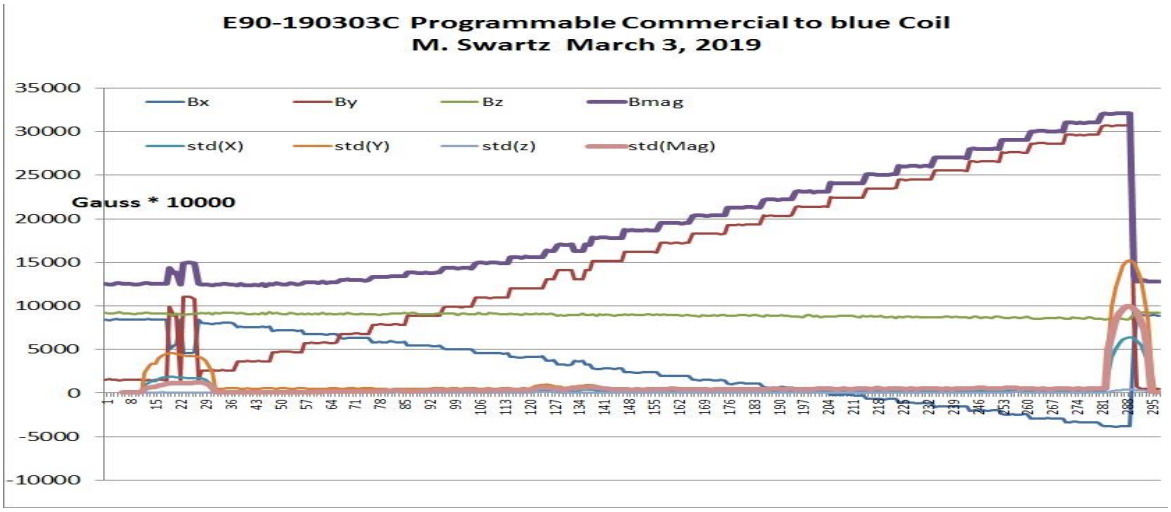

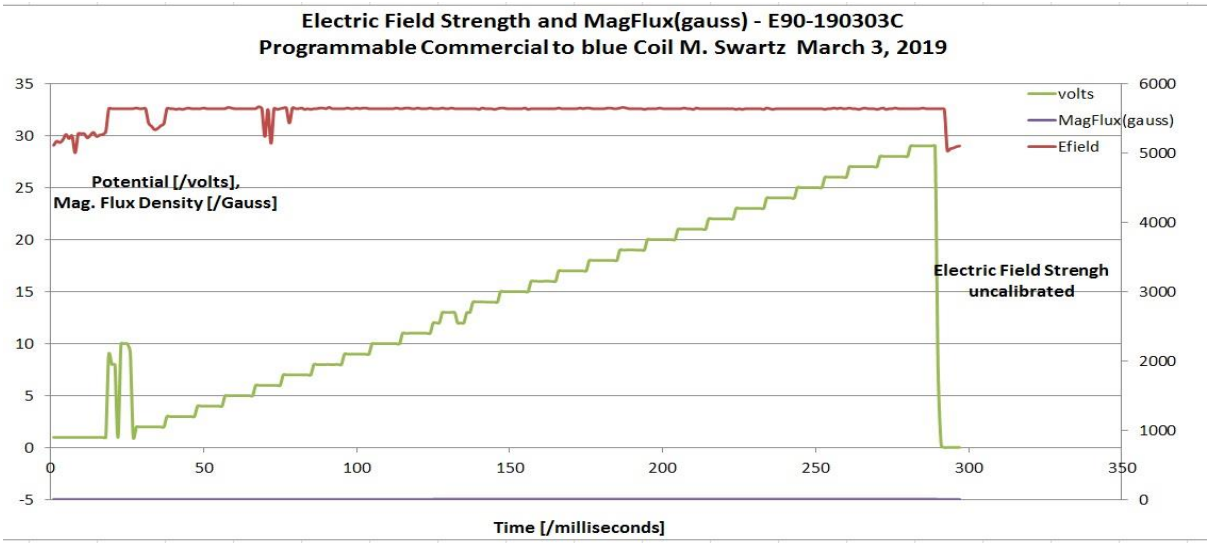

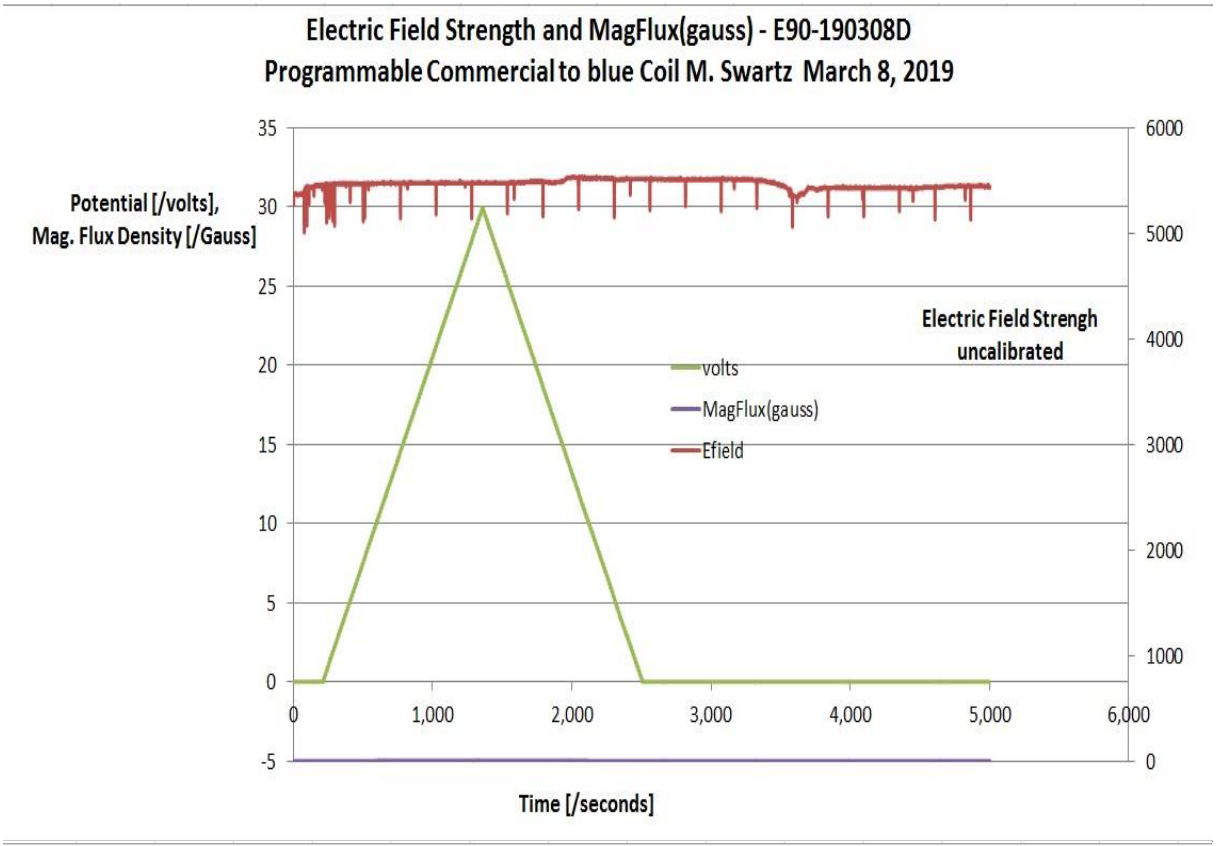
Electric Field Strength and MagFlux(gauss) - E90-190308D
Programmable Commercial to blue Coil M. Swartz March 8, 2019
Potential [/volts],
Mag. Flux Density [/Gauss]
Electric Field Strengh
uncalibrated
volts
MagFlux(gauss)
Efield
Time [/seconds]

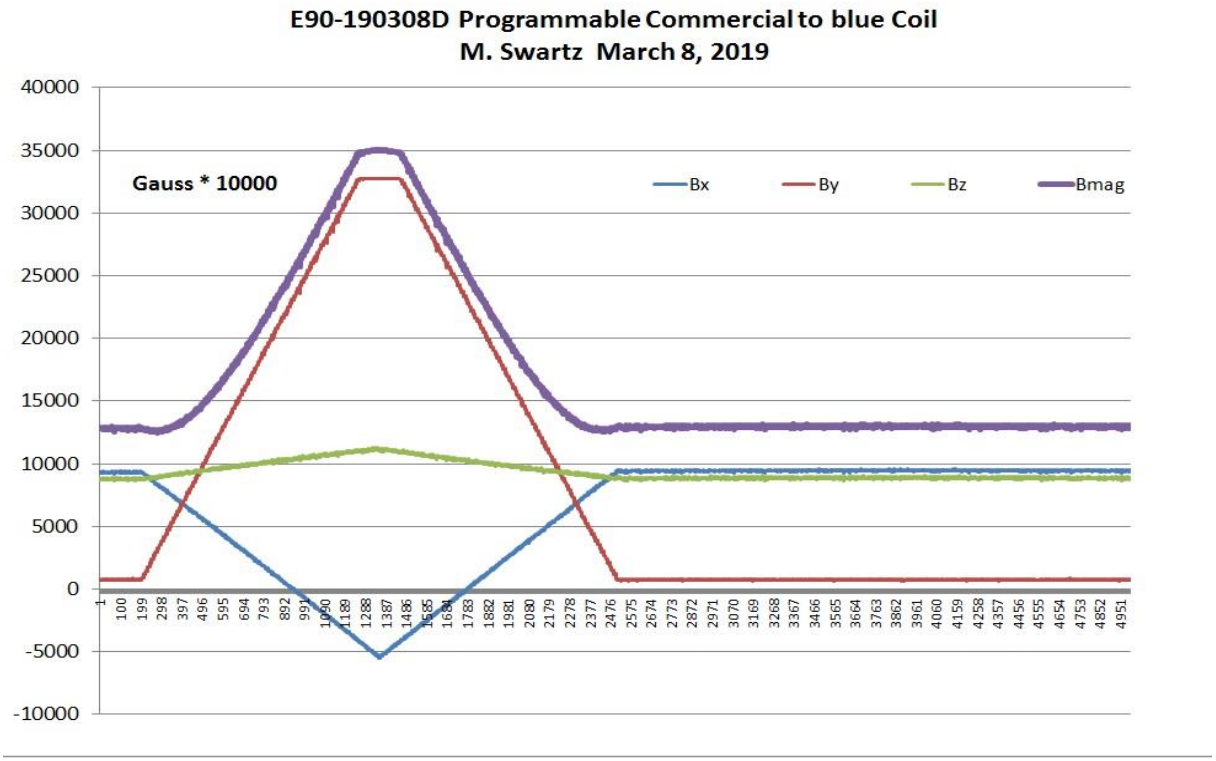
E90-190308D Programmable Commercial to blue Coil
M. Swartz March 8, 2019
Gauss * 10000
Bx
By
Bz
Bmag

Figure 11-12

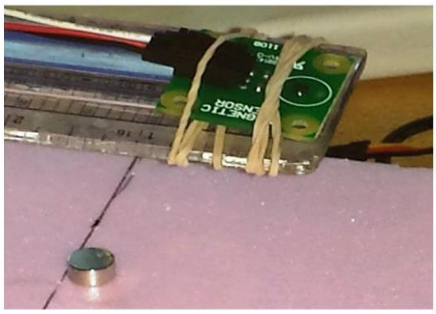

Wednesday, February 12, 2020 Nanortech Inc. Proprietary and confidential © Dr. Mitchell Swartz 2016

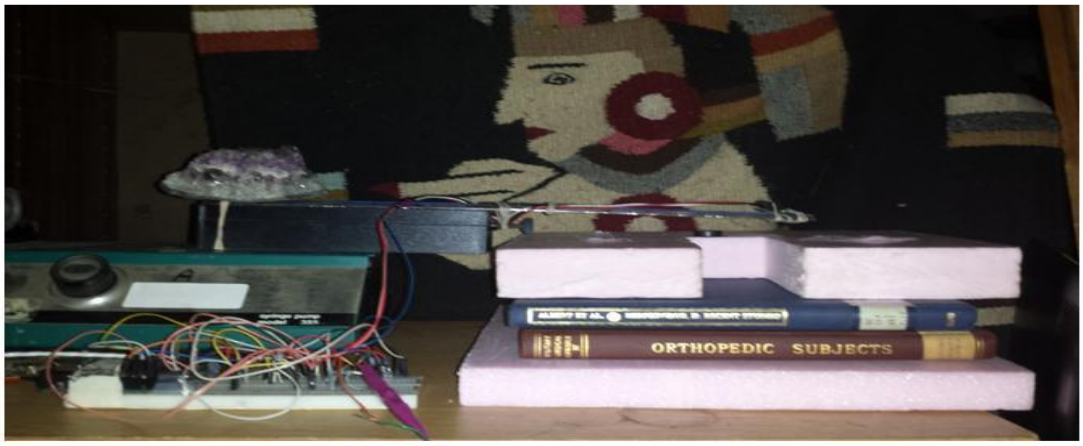

Wednesday, February 12, 2020 Nanortech Inc. Proprietary and confidential © Dr. Mitchell Swartz 2016

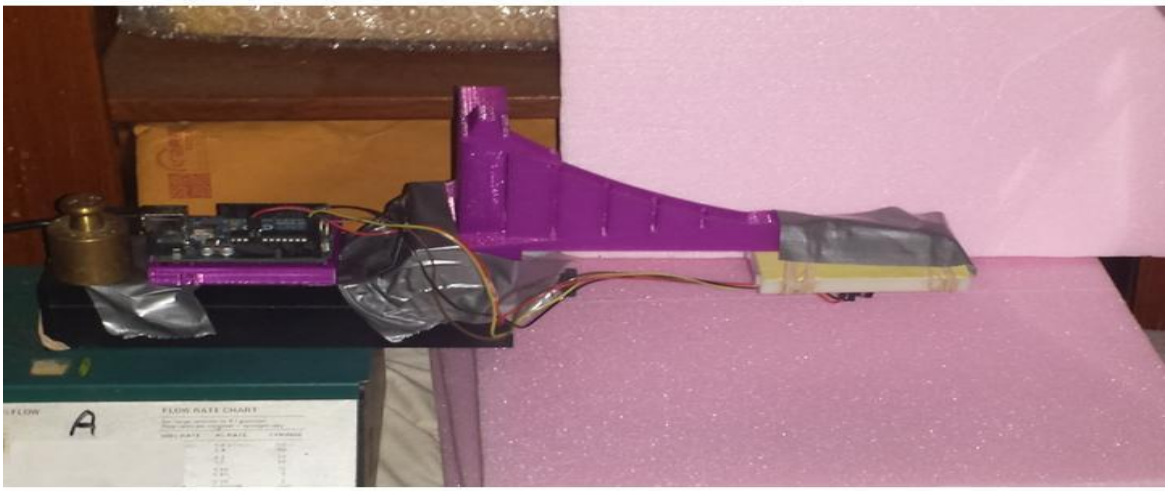

Wednesday, February 12, 2020 Nanortech Inc. Proprietary and confidential © Dr. Mitchell Swartz 2016

Figure 13 -15

NANOR 7-10

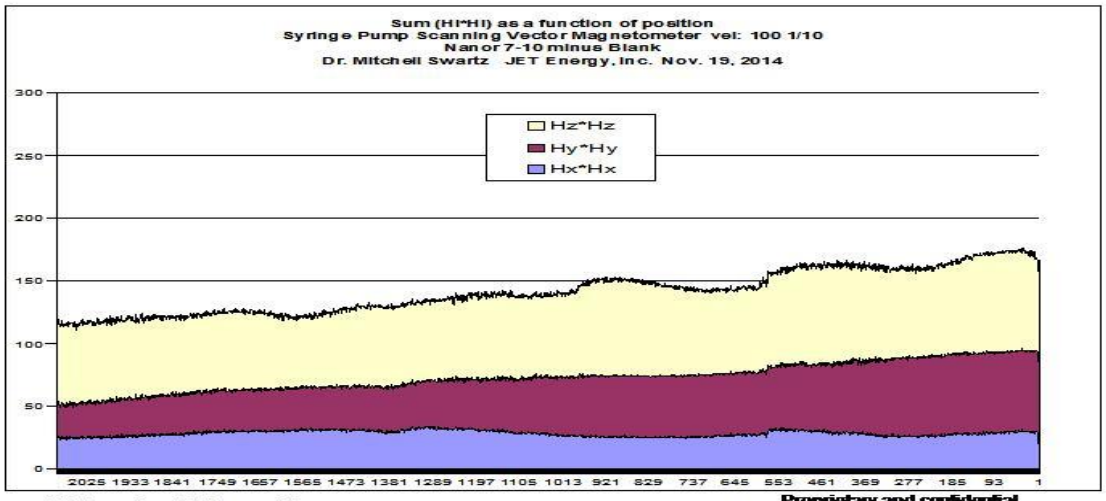

NANOR 7-23

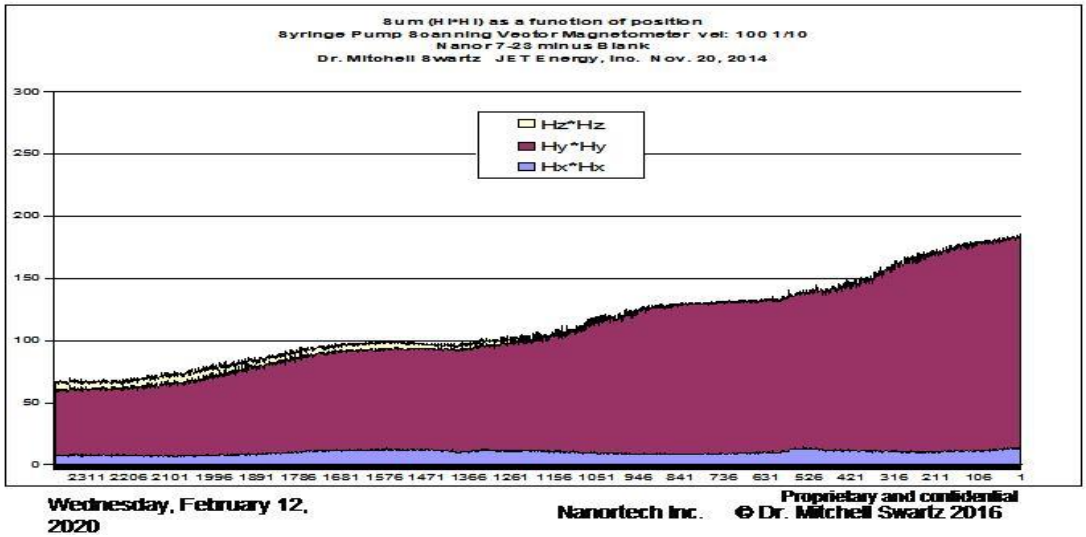

Figure 16-17

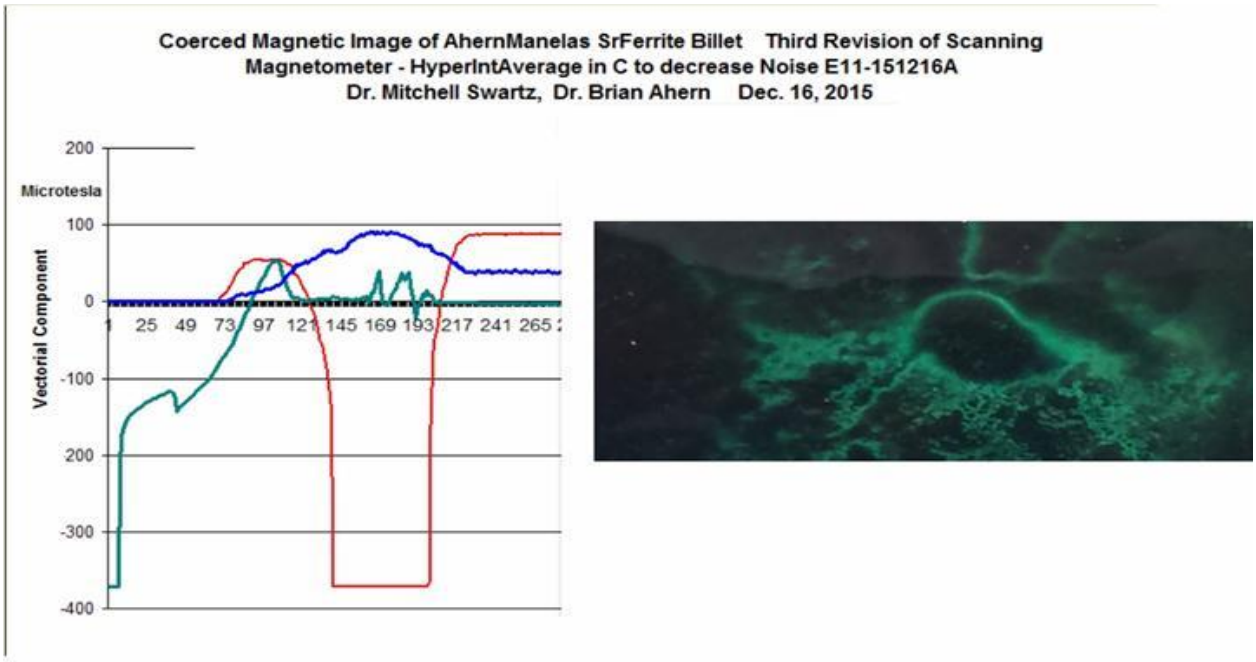
Coerced Magnetic Image of AhernManelas SrFerrite Billet Third Revision of Scanning
Magnetometer - HyperIntAverage in C to decrease Noise E11-151216A
Dr. Mitchell Swartz, Dr. Brian Ahern Dec. 16, 2015
Microtesla
Vectorial Component
200
100
0
-100
200
-300
-400
1 25 49 73 97 121 145 169 193 217 241 265
Wednesday, February 12, 2020
Nanortech Inc.
Proprietary and confidential
© Dr. Mitchell Swartz 2016

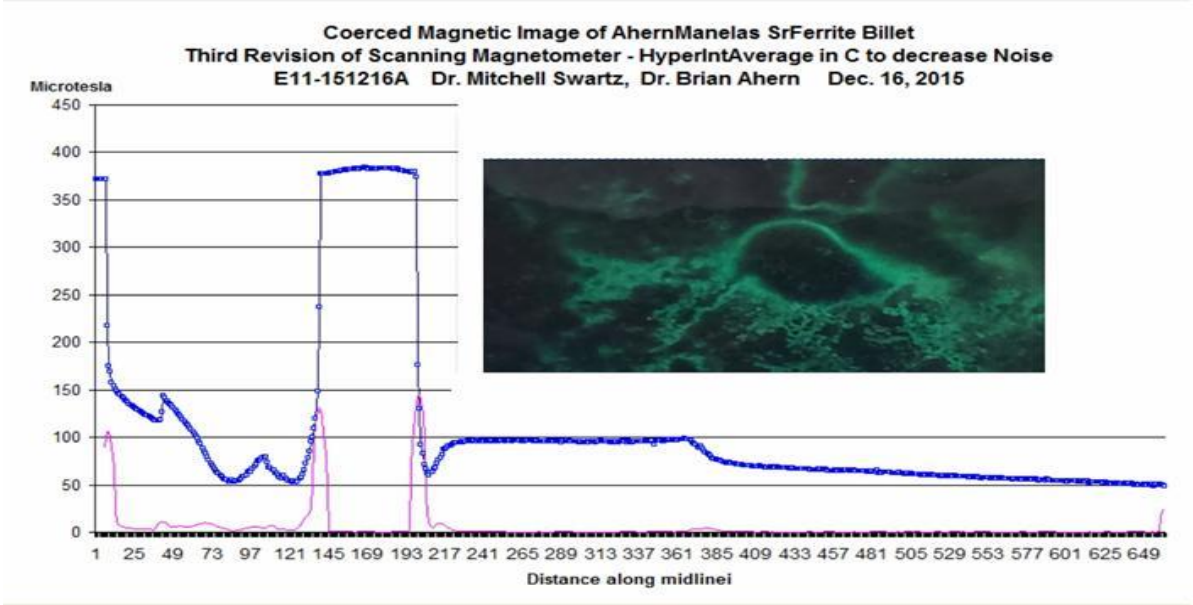
Coerced Magnetic Image of AhernManelas SrFerrite Billet
Third Revision of Scanning Magnetometer - HyperIntAverage in C to decrease Noise
E11-151216A Dr. Mitchell Swartz, Dr. Brian Ahern Dec. 16, 2015
Microtesla
450
400
350
300
250
200
150
100
50
0
1 25 49 73 97 121 145 169 193 217 241 265 289 313 337 361 385 409 433 457 481 505 529 553 577 601 625 649
Distance along midlinei
Wednesday, February 12, 2020
Nanortech Inc.
Proprietary and confidential
© Dr. Mitchell Swartz 2016

Figure 18 -19

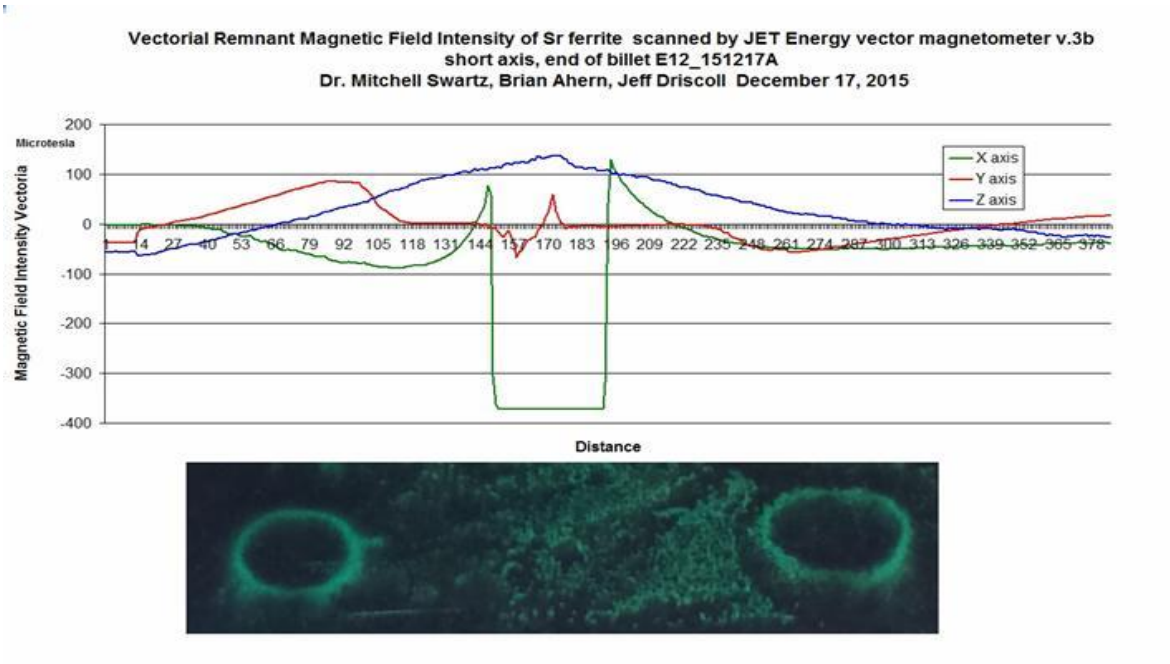

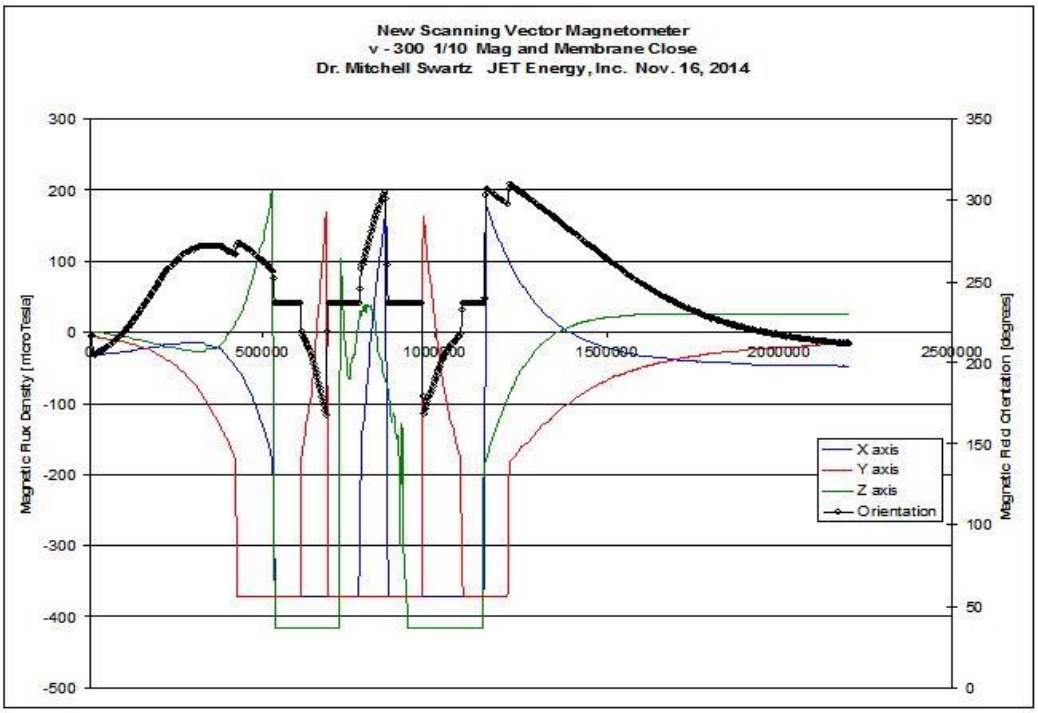

Figure 20-21-

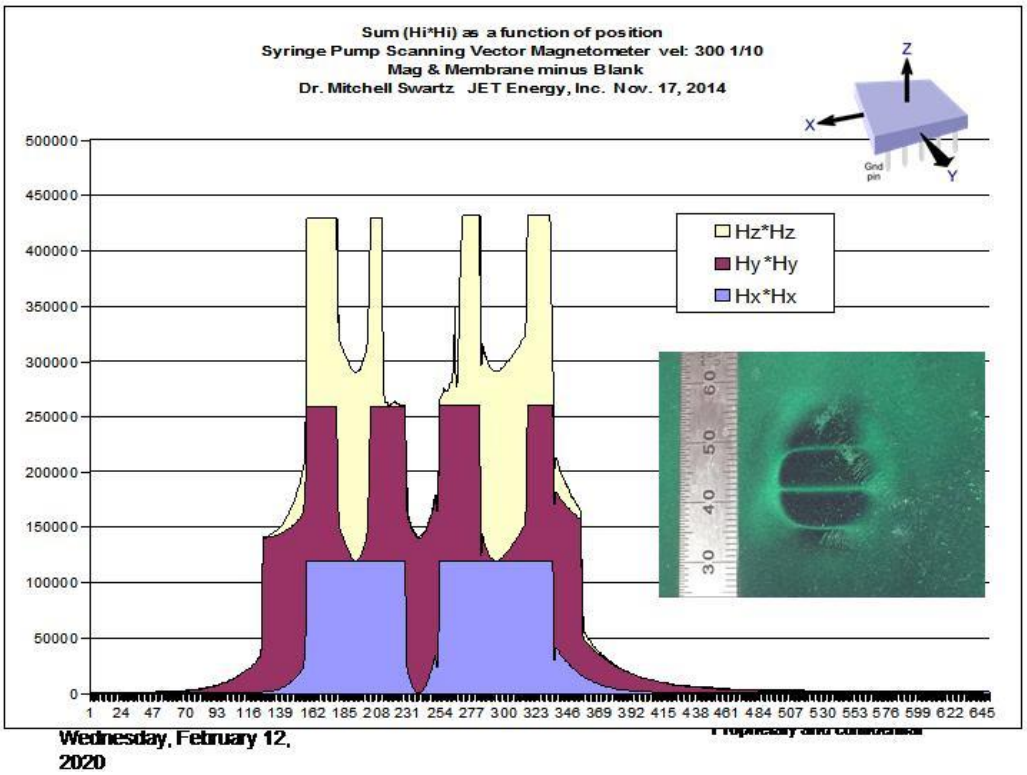

Figure 22 -

9. Introduction - NANOR®-type CF/LANR dry preloaded components

A NANOR-type component is a hermetically sealed CF/LANR [cold fusion/lattice assisted nuclear reaction] nanomaterial, preloaded and arranged as a two-terminal electrical component which can yield significant heat [Figures 1,2]. They are designed to avoid leakage, and enable stabilization and activation of the contained nanostructured alloyed material. As a result, the NANOR®-type preloaded component [1,2] has been like the proverbial "lab rat" for several papers, and was also the central component in an open demonstration at MIT in 2012 [3; which is one of the locations where the "normal" (unexposed to magnetization effects) exponential fall off of CF/LANR activity was followed over months]. The papers include investigations of material science [4-6] and radiation physics [5,6,8], which have revealed several electrical transconduction states. Most importantly, of these transconduction states, only one produces the desired trait known as "excess heat" [7]. We begin by considering how the activity of these components is measured, and then how they are affected by the applied magnetic field intensity, and finally what may cause the post-magnetic activity-oscillations.

10 Methods – Determination of Activity of NANOR®-type Components

The preloaded NANOR®-type components are driven by a high voltage circuit (up to 3000 volts peak). In addition to using several types of commercial calibrations, we augment the calibrations using Keithley picoammeters (Types 480 and 486) and Keithley current sources (Type 225). For voltage measurements, Keithley electrometers (610B,610CR,602) and HP5334, HP3490, and Keithley multimeters were used. Voltage sources include HP-Harrisons, Kepco, and VWR. The input voltage was delivered in every run alternatively to the NANOR and the ohmic control which was at the same location and used to thermally calibrate the system [9-11].

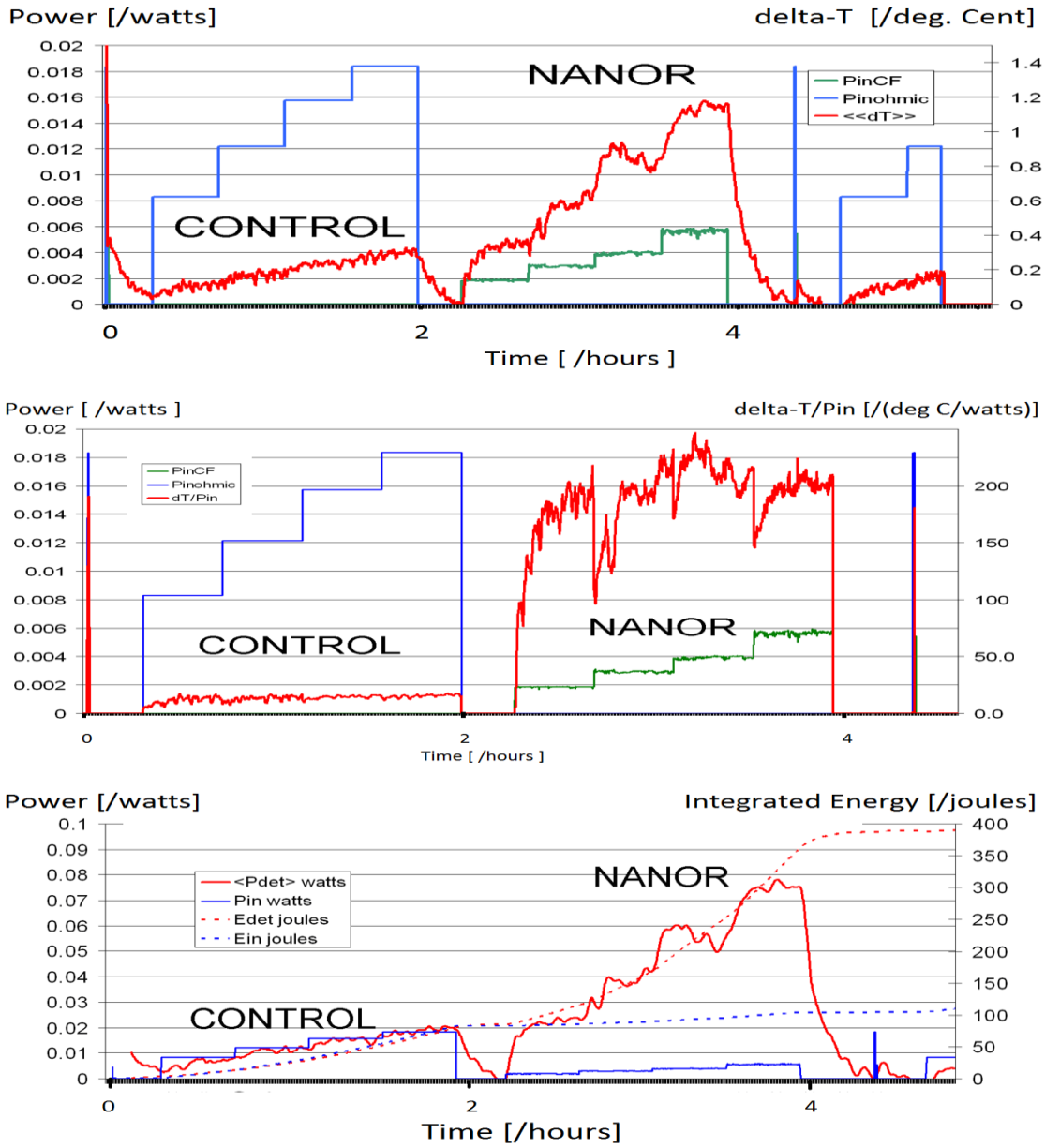

Fig. 23 – Response of a Control and NANOR®-type Component – No Magnetic Field
This figure shows three different ways of evaluating the possible presence of excess energy from a single run of an ohmic control and a NANOR®-type component. The ohmic control was driven first and then the component was electrically driven, as marked.
[top] The electrical input power and resultant delta-T for the ohmic control and then the NANOR®-type component are shown. [middle] The electrical input power and resultant delta-T normalized to the input power [delta-T/Pin]. Importantly, this linearizes the output and enables calculation of power gain. In contrast to the graph on the top, this metric is a nearly straight horizontal line for the ohmic control. [bottom] Calorimetric presentation of the input power and energy and output power and heat for the ohmic control and the NANOR®-type component.

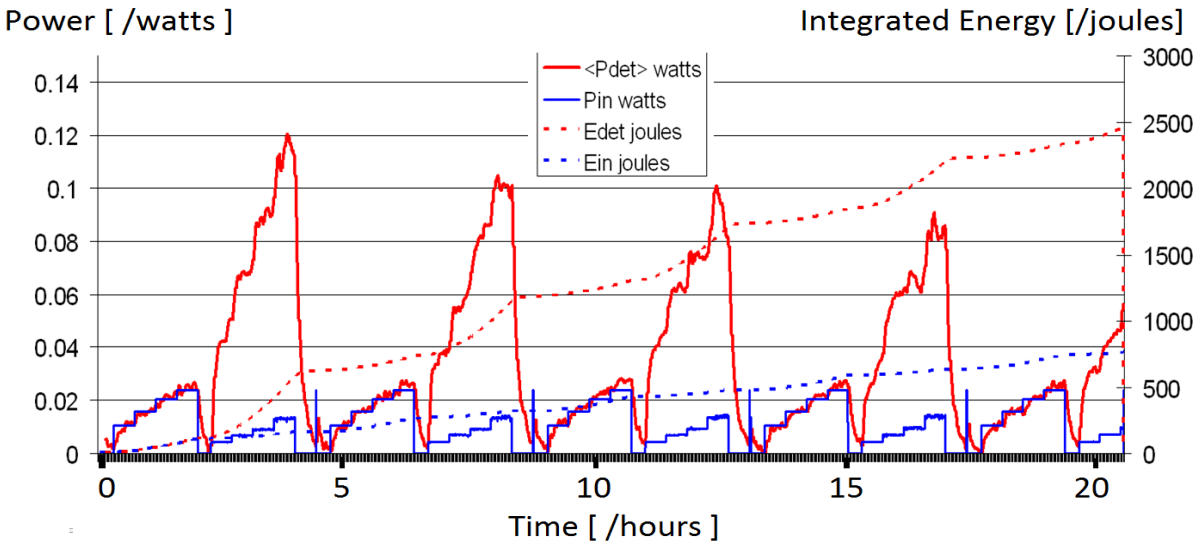

Fig.24 – Reproducibility of a NANOR®-type component – No Magnetic Field
This is a calorimetric presentation of an experimental run, discontinuous with Fig. 3, with more than four cycles. The electrical input power and energy and output thermal power and heat are shown alternatively both from the ohmic control and the NANOR®-type component at several input powers. This component and control had NOT been driven in the presence of an applied magnetic field intensity, unlike Figures 3 and 4.

Input power is defined as V*I. There is no thermoneutral correction in the denominator. Therefore, because consideration of loss by possible recombination is not removed, the observed power is a lower limit [12]. The energy calculations are also calibrated by time integration for additional validation. The instantaneous power gain [non-dimensional power amplification factor; 10.11,13] is defined as P_{out}/P_{in}. When present, the excess energy is defined as [$P_{output} - P_{input}$] * time. Data acquisition is taken from voltage and current sensors, and temperatures and heat flux sensors at multiple sites of the system. Data sampling is at 0.20 Hertz to 1 Hertz, with 16-24^{+} bit resolution, a voltage accuracy of $0.015^{+/-0.005}$ volts, and a temperature accuracy of <0.6 degrees C. The noise power of the Keithley current sources driving the reactions is generally ~10 nanowatts.

After driving the component and the control in each run, their power and energy gain were separately determined both by power-normalized delta-T (dT/ P_{in}), and input power normalized increase in heat flow (delta-HF/P_{in}), and the directly by semiquantitative calorimetry [2,3]. In semiquantitative calorimetry, the amount of output energy is directly determined from the heat release, which is then compared to the input energy. The 'excess heat'-producing activity can be determined by comparing the output of the NANOR® type component to the output of the precisely-driven ohmic control, as demonstrated in the middle of Figure 1.

11. Methods – Magnetization of NANOR®-type Components

For what is reported here, the applied magnetization sequence consisted of rapidly repeating pulses of an intense >2 Tesla magnetic field intensity [4]. The applied magnetic field intensity, thus, highly-fractionated with 3500 pulses delivered, each with a rise time of <0.1 millisecond, followed by an intra-pulse delay of one second.

12 Results – Response Without Applied Magnetic Field

Fig. 1 shows the response of these CF/LANR NANOR®-type components with any applied magnetic field intensity in three graphs of the same experimental run. A determination of the presence of excess heat can be made by comparing the output for NANOR®-type LANR component to the thermal (ohmic) control. The top of Figure 1 shows the electrical input power and the incremental output temperature rise [defined as "delta-T"]. The x-axis represents time. The y-axis on the left side represents electrical input power in watts. The y-axis on the right side represents delta-T. The calibration pulses, used for accuracy and precisions checks of voltages and currents and time, are also shown. The middle of Figure 1 includes the same data but the incremental output temperature rise is normalized to the input power by dividing by the input power. This metric has delta-T/Pin be a nearly straight horizontal line for the ohmic control; which facilitates semiquantitative measurements by use of a simple ratio. The bottom of Figure 1 is a full calorimetric presentation showing the input power and energy and output power and heat (energy) from the ohmic control and the NANOR®-type component at several input powers. The y-axis on the left side represents electrical input power in watts. The y-axis on the right side is the time-integrated amount of energy delivered at input, and then released. The lighter energy curves (dots) are read off of the right hand y-axis, which represents the amount of energy released in joules.

These calorimetric curves thus rule out energy storage, chemical sources of the induced heat, possible phase changes, and other sources of possible false positives.

Figure 2 shows the calorimetric responses of both the ohmic control and the preloaded NANOR®-type component over four complete cycles, at four different input electrical power levels. Figures 1 and 2 show that the active preloaded CF/LANR component has significant improvement in thermal output compared to a standard ohmic control (a carbon composition resistor). They also demonstrate that excess heat was produced only during energy transfer to the NANOR®-type LANR component heralding clearly over-unity thermal output power from it. Figure 2 demonstrates the reproducibility of the ohmic control and the near reproducibility of the NANOR®-type component over several cycles. In Figure 2 the peak power gain of the NANOR®-type component slowly decreases, in a regular way, over time. It looks like it could be linear or exponential.

Figure 2 also demonstrates an exponential falloff of the peak incremental excess power gain. It is important to note that this component had NOT been driven in the presence of an applied magnetic field intensity, versus what is shown in Figure 3. Contrast this exponential, slowly decreasing response, which is what was always seen [1-5], to the newly observed irregular, somewhat oscillatory-like, activity which occurred only after the components were exposed to the H-field, and only while an applied E- field was used to activate the CF/LANR component (Figs 3 and 4).

13 Results – Unique Response After Magnetic Field

Introduction - Magnetic Responses in CF/LANR Systems

Previously, magnetic [14-16] and radiofrequency electromagnetic [17] effects have been reported in aqueous CF/LANR systems. In aqueous CF/LANR systems, steady magnetic fields have a small inhibitory effect on loading electrolysis when the applied H-field is perpendicular to the direction of the electrical currents [16]. In dry, preloaded CF/LANR systems, at higher electrical drive currents to the component, time-varying alternating magnetic fields simultaneously applied, induce small to significant increase gains in the activity [4] and some changes are long-lasting. Therefore, magnetically treated NANOR®-type components are called M-NANOR®-type components to distinguish them and anticipate their unique oscillating-activity behavior and other longer term effects (Figures 3,4).

14 Synchronous Magnetically-induced Increased Energy Gain

During the first magnetic-NANOR run, we were quite surprised by the different responses of the NANOR component during and after dH/dt coercing. Astonishingly, it was discovered that for magnetic interactions with active nanostructured CF/LANR systems [4], there is enhanced improvement of LANR (which occurs at the same time as the magnetization and therefore is called "synchronous"). As a result of the magnetization sequence, there appeared a remarkable increase in incremental power gain and excess energy gain, over ordinary CF/LANR. This magnetization sequence created an increase of circa 4 to 10 times the peak power gain over conventional LANR with the same system. The peak power gain of such treated NANOR®s ranged from 22 to up to ~80 times input electrical power or more beyond the control, as determined by calorimetry [4,10,11].

There are also subsequent effects (occurring later, or metachronous) and strong evidence for the first ever-observed two (2) optimal operating point (OOP) manifolds [4]. Some of these dramatic changes can be seen in Figure 3 which shows the first evidence of magnetic rejuvenation of nanostructured CF/LANR material, and even increasing the CF/LANR activity to higher levels than observed initially!

Figure 3 shows a calorimetric presentation of the ohmic control and the NANOR®-type component. It demonstrates the impact of the magnetic field, with no change from the same magnetic field on the background or control. In Figure 3, the magnetic field intensity was applied only at one point in time which is indicated by the black arrows. At all other points in time, there was NO additional applied magnetic field intensity. Note the synchronous amplification of the M-NANOR power output induced by the magnetic field. This is not seen in the ohmic control.

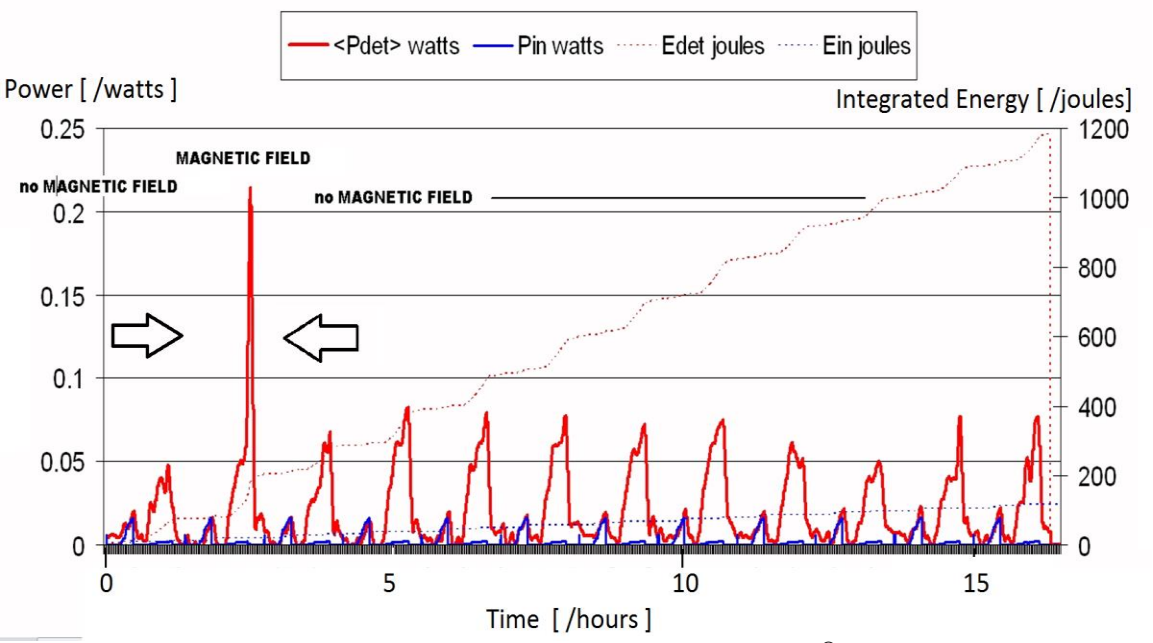

Fig. 25 – Impact of an H-Field on the Behavior of a NANOR®-type Component

This experimental runs shows the impact of an applied H-field on the activity of a NANOR®-type component before, during and after, a single sequence of fractionated high intensity magnetic field application between the arrows. At all other points in time there were NO additional large applied magnetic field intensity. Note the absence of an exponential or linear fall-off of peak activity.

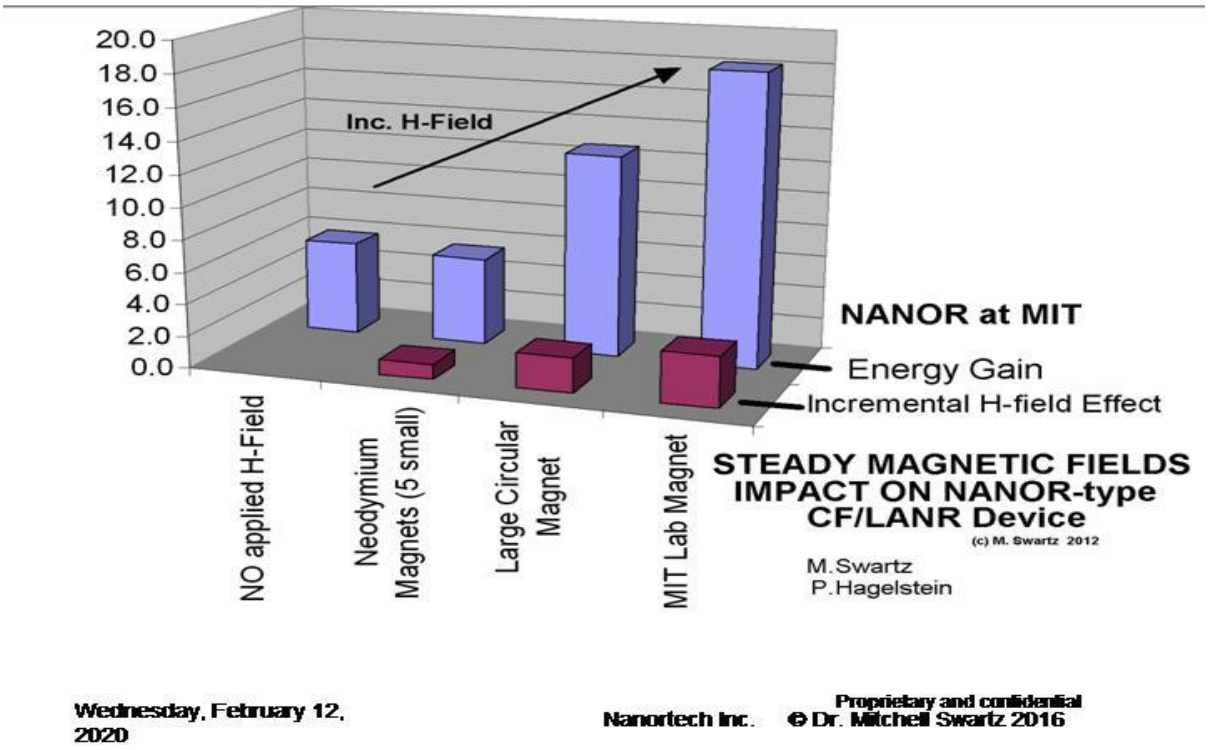

Figure 26 -

15. Metachronous Magnetically-induced Increased Energy Gain

Other effects were noted. Astonishingly, after the single application of the fractionated large applied magnetic field intensity was delivered at one point in time (between the arrows), there is improvement in the CF/LANR activity which also appears later - long after the initiation of the magnetization [4]. This metachronous impact wrought upon the treated CF/LANR M-NANORs, long after the treatment, is heralded as increased power and energy gain as determined by delta-T/P_{in}, delta-HF/P_{in}, and calorimetry. Subsequent, metachronous effects are those physical changes wrought by the applied high intensity fractionated magnetic field after the field was applied.

Figure 4 is a calorimetric presentation of a different run later many hours after the single application of the fractionated large applied magnetic field intensity was delivered. In Fig. 4, many cycles are shown which demonstrated clearly that there was more output than the ohmic control, and as astonishingly, there is improved activity which is shown here to be metachronous and long-lasting. Notice that the peak power gain of the M-NANOR®-type component is increased **after** the application of the fractionated large applied magnetic field intensity.

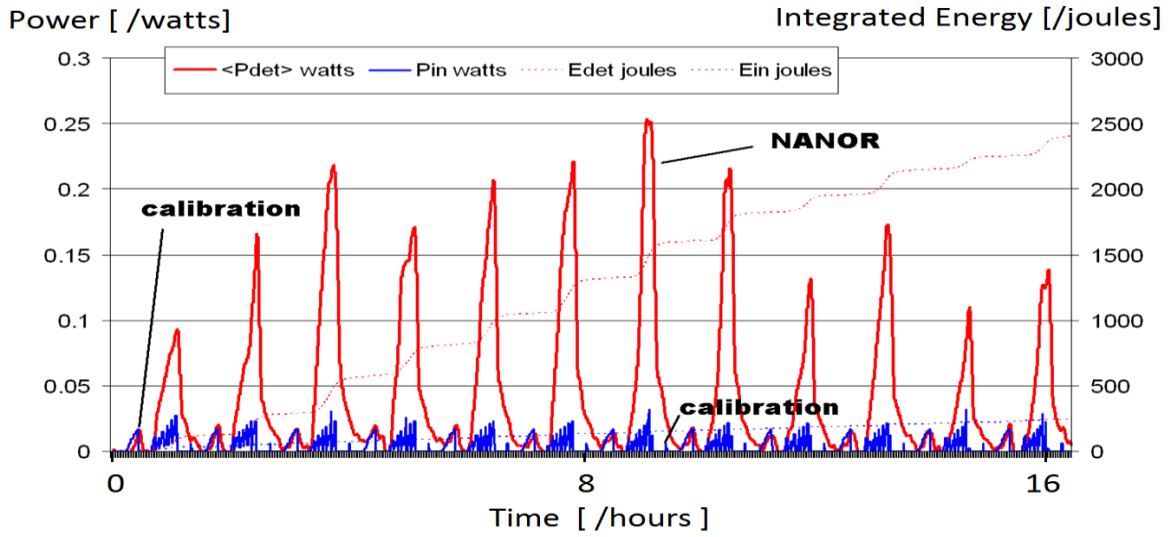

Fig. 27– Subsequent Late-term Impact of Magnetization on CF/LANR Activity

The post-magnetization electrical input power and energy and output power and heat are shown for the ohmic control and the NANOR®-type component. This experimental run of a M-NANOR®-type component was made several hours after a single application sequence of the fractionated magnetic field was delivered. There was no additional H-field applied for this figure. The peak applied voltage was ~125 volts. Note the absence of an exponential or linear fall-off of peak activity.

16. Magnetically-induced Activity Has an Oscillation of Activity

There are other remnant effects long after the application of the H-field. These late-appearing effects include an increased, but variable, activity. The subsequent activity of the magnetized M-NANOR®-type components no longer decreases in a simple regular, evanescent manner over time [as described in previous publications; 1-5] but instead appears irregular with a periodic component, as first seen in Fig. 3 and also shown in Fig. 4. The cyclic component of the activity in in the range of circa 1.3×10^{-4} Hz [$0.2\text{-}5 \times 10^{-4}$ Hz].

17. Magnetically-induced Unique Dual Optimal Operating Manifolds (OOPs)

Although not covered in detail here, previously, all CF systems and the NANOR®s had shown a single optimal operating point manifold for excess heat operation, ^{4}He production, and other products [15,14,4]. Today, that is no longer accurate. Even after a single treatment to a high intensity fractionated magnetic field, there arise two OOP manifolds. The new OOP is elicited at higher input electrical power, and so the new, second, OOP is located to the "right" of the conventional, first, CF/LANR OOP [4]. Although this revelation is far beyond the scope of this paper, its impact is very important because magnetically activating preloaded nanostructured CF/LANR devices is both very useful [4] and instructive [8]. Although cold fusion (LANR) has a first stage mediated by phonons within the loaded lattice by coherent Phusons [18], there is also a magnetically coerced second stage, which we believe may be mediated by magnons, or interactions of phonons in H-field and included magnetization field.

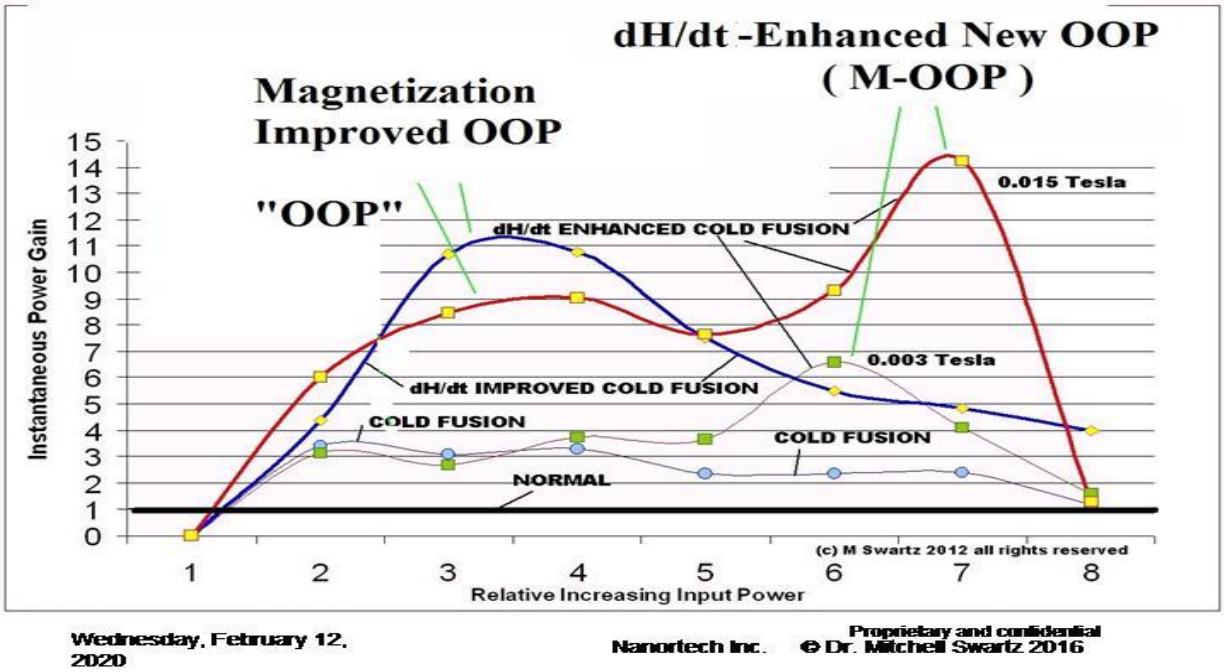

Figure 28 -

18 INTERPRETATION – Possible Implications of Magnetized Domains

The unique temporal changes, shown in Figures 3 and 4, and the amplification of CF/LANR excess heat by fractioned magnetic fields effects suggest a new CF/LANR material science/nuclear interaction. The analysis below is thus important because the magnetic domains, magnetic interactions, magnetically-increased incremental power gain, might be relevant to other materials and other systems.

19 INTERPRETATION – Magnetism in ZrO_2-Pd/Ni and ZrO_2-Pd Components

How can palladium become magnetic? Nickel is ferromagnetic and the induction of magnetization is to be expected. So this is expected for the nickel-containing NANORs, but it is somewhat surprising for the palladium M-NANORs. However, palladium like platinum, has potential capacity as an exchange-enhanced paramagnetic materials to exhibit a strong Stoner enhancement and become ferromagnetic upon tension [19]. When the Stoner criterion is

satisfied, in response to external stimuli such as applied E-field, the materials can exhibit unconventional magnetic responses -- they become exchanged-enhanced ferromagnetic.
Thus, the solid state metallurgical lattice of Pd can become ferromagnetic or its equivalent post-magnetization. This has now been seen [20] and confirmed in magnetic domain scanning and imaging which will be the subject of an upcoming paper (confer also Figure 5).
The magnetization and oscillations may also be consistent with other reports of quantum oscillations in several systems, including metallic triangular-lattice antiferromagnet $PdCrO_2$ [21], and as seen in the (electrically-tunable) anomalous Hall effect observed in platinum thin films [22], as seen with both lattice and magnetic oscillations in stacks of Josephson junctions [23], and with reports of excess energy production with high voltage magnetic pulses coerced through nanograined magnetic materials such as strontium ferrites [24]. The coerced magnetization is important and may also be consistent with some of those materials considered theoretically in investigations using DFT calculations of strained ferromagnetic lattices [25].

21 INTERPRETATION – Interaction Forces between Magnetized Domains

It is important to consider the material science and metallurgy of this new magnetic behavior and material(s) (Figure 5). From what do the domains arise, and how do they interact. How can the magnetic domains couple and account for the unusual time-variant activity? Magnetic materials can self-interact, as described by the Langevin function [26]. Theoretically, this is supported by density-functional calculations [27]. Most interestingly, this appears to be driven by vacancies in Pd (theoretically, up to 15% calculated using the SCR Korringa-Kohn-Rostoker coherent potential approximation method, which predicts a magnetic moment at ~10% vacancies) [28]. Attention is drawn to the interesting fact that several theories of cold fusion also require vacancies [29].

22 NEW HYPOTHESIS – Is Oscillation of Activity Linked to Magnetized Domains

The continuum electromechanical equations may give a possible new understanding of the just-discovered time-varying activity change that appears in post-magnetized components [4]. This is important because these changes are uniquely different from observations of hundreds of runs on scores of samples. These M-NANOR®-type components have responded markedly differently, requiring this attempt to mathematically analyze, and possibly explain, this new post-magnetization observation. The activity oscillations observed in the output excess power of M-NANOR®-type components long after their magnetic field interaction must result from the applied magnetic field intensity. So what is the impact of the H-field on any magnetic domains there? We have begun to measure them in M-NANORs after magnetization [20] as shown in Figure 5.
In this report, we examine the behavior of the oscillating excess heat activity of magnetized M-NANOR-type components, and attempt to link that behavior to loco-regional magnetic domains in the treated coerced lattice to understand the very unique observed responses of these magnetically treated components. Although better models for, and a solution to, this observation are needed, this is a first approximation.
These domains can be modeled as a remnant magnetization of the lattice, and here are taken into account through the forces and tension they incur through the density of the lattice and Poisson's ratio. Specifically, using the findings of strained layer ferromagnetism in transition metal, it is found that tension increases magnetization and simultaneous should decrease density [25], and these may be the conditions that give rise to the activity oscillations.

23 Magnetic Forces and Oscillations from CF/LANR Domains

To model the interactions of two neighboring magnetic domains, we assume that in addition to the normal mechanical restoring forces that there are also electromechanical forces. We begin the analysis with Newton's equation, using a continuum model using a simple spring constant equation for the initial analysis.

$$\frac{(d^2x)}{(dt^2)} = \frac{F}{M} \qquad \text{[Eq. 1]}$$

The magnitude of the restoring force is derived using Hooke's law augmented by the Maxwell Stress tensor which is integrated over the surface boundary between those two magnetic domains to derive the volume-integrated induced force [30-32].

The force density, in integral and differential forms, thus becomes

$$\int_V \left[-\tfrac{1}{2}\mathbf{H}\cdot\mathbf{H}\,\nabla\mu + \nabla\left(\tfrac{1}{2}\mathbf{H}\cdot\mathbf{H}\frac{\partial\mu}{\partial\rho}\rho\right) - \mathbf{F}\right]\cdot\delta\boldsymbol{\xi}\,dV = 0$$

$$\mathbf{F} = -\tfrac{1}{2}\mathbf{H}\cdot\mathbf{H}\,\nabla\mu + \nabla\left(\tfrac{1}{2}\mathbf{H}\cdot\mathbf{H}\frac{\partial\mu}{\partial\rho}\rho\right) \qquad \text{[Eqs. 2,3]}$$

Therefore the force, and the stress tensor, would there be, and derived as follows:

$$F_m = \frac{\partial T_{mn}}{\partial x_n}$$

$$T_{mn} = \mu H_n H_m - \tfrac{1}{2}\delta_{mn}H_k H_k\left(\mu - \frac{\partial\mu}{\partial\rho}\rho\right) \qquad \text{[Eqs. 4,5]}$$

$$M\frac{d^2x}{dt^2} = -[\mathrm{K}*\mathrm{x}] - \frac{[Bo]^2}{2*\mu^2}\left[\Delta\mu + \left[(-\Delta\rho)*\left(\frac{\delta\mu}{\delta\rho}\right)\right]\right] \qquad \text{[Eq. 6]}$$

The solution has an amplitude of

$$\frac{[Bo]^2}{2*V*\rho*\mu^2*K*\sqrt{(\omega_0{}^2-\omega^2)}}*\left[\Delta\mu + \left[(-\Delta\rho)*\left(\frac{\delta\mu}{\delta\rho}\right)\right]\right] \qquad \text{[Eq. 7]}$$

and a natural frequency of

$$\omega_0 = \sqrt{\frac{K}{\rho*V}} \qquad \text{[Eq. 8]}$$

This might be the resultant natural frequency which we see in the M-Nanor's excess energy cyclic activity (confer Figures 3 and 4).

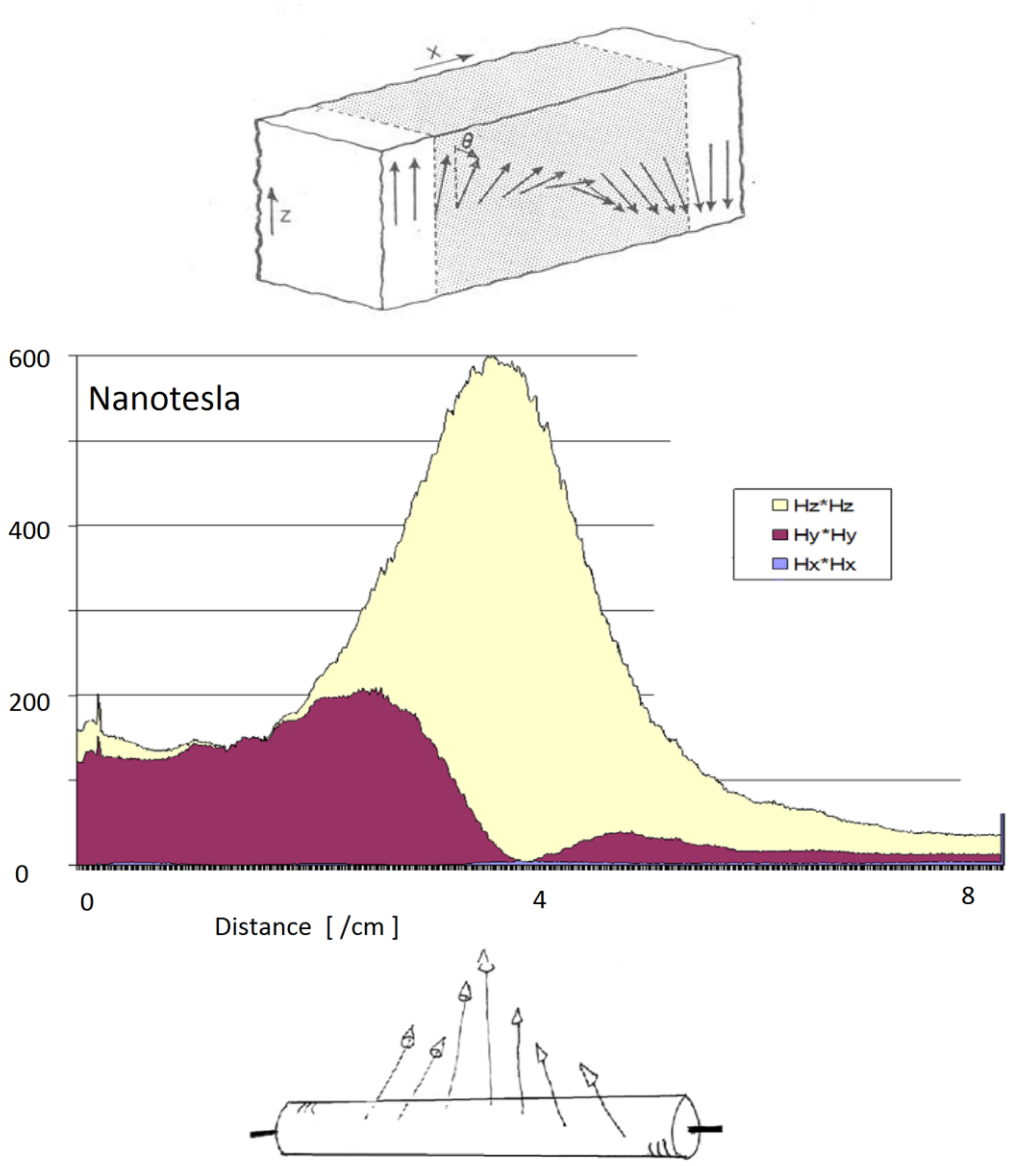

Figure 29 – Magnetic Domains in NANOR-type components
(top) Schematic showing magnetic domains interacting within a lattice. The magnetization is observed changing over a distance (after John Mara and A.von Hippel [32]. (bottom) These magnetic domains have been observed experimentally and their imaging, and possible implications, are the focus of a manuscript [20]. The graph shows the vectorial scanned magnetization from the domain (in nanotesla) as a function of distance along the long axis of the M-NANOR 7-8 at rest, long after it was previously operated. The square of each of the x-, y-, and z-axis components are shown as a function of x-axis. (bottom inset) Estimated vectorial magnetization along, and just vicinal to, the body of M-NANOR 7-8.

Note the magnetoelectric term at the end (reminiscent of electrical dielectrophoresis). Substitution in the original equation, with terms including magnetostriction, gives

24 CONCLUSION - Oscillating Activity and Magnetic Domains

There are two types of NANOR-type CF/LANR components. They have very different behavior. The post-magnetization effects are significant and time-variant because it has now been discovered that high intensity, dynamic, repeatedly fractionated, magnetic fields have an incremental major, significant and unique, complex, metachronous amplification effect on preloaded M-NANOR®-type LANR devices.

Furthermore, in contrast to previously-observed exponential falloffs of sample activity [peak incremental excess power gain], post-magnetization activity demonstrates oscillatory activity, and the Maxwell stress tensor heralds a theoretical frequency for oscillations now observed to exist between these magnetic domains in these magnetized NANOR®-type components. The observed frequencies of activity change observed appear be circa 1.3×10^{-4} Hz [range $0.2\text{-}5 \times 10^{-4}$ Hz].

This paper's analysis of the force density, calculated by using the Maxwell stress tensor, predicts oscillations now observed to exist between these magnetic domains in these magnetized NANOR®-type components. This analysis indicates that magnetic interactions between domains should augment other restoring forces, and that the frequency should increase with decreasing mass, and increasing applied magnetic field intensity (presumably until coercion effects elicit no further increase). It is important to consider this new material science and metallurgy with surprising new magnetic behavior in future analyses and experiments.

Acknowledgments

The author acknowledges and thanks Gayle Verner for her very helpful editorial support. The author is grateful to and thanks the teams who have helped collect the data, support the work, and have helped better understand the physics and materials with their assistance, ideas and suggestions including Gayle Verner, Alex Frank, Alan Weinberg, Charles Entenmann, Allen Swartz, Isidor Straus, Joshua Gyllinsky, Peter Hagelstein, Florian Metzler, Brian Ahern, Jeff Driscoll, Dennis Cravens, Pamela Mosier Boss, Lawrence P. Forsley, Frank Gordon, Louis DeChiaro, and Dennis Letts. This effort was supported by JET Energy Inc. and the New Energy Foundation. NANOR® and PHUSOR® are registered trademarks of JET Energy, Incorporated. NANOR®-technology, and PHUSOR®-technology are protected by U.S. Patents D596724, D413659 and several other patents pending.

References

[1] M.R. Swartz, G. Verner, J. Tolleson, P. Hagelstein, **Dry, preloaded NANOR®-type CF/LANR components**, *Current Science*, 108, 4, 595 (2015).

[2] M.R. Swartz, Hagelstein P.I., **Demonstration of Energy Gain from a Preloaded ZrO_2–PdD Nanostructured CF/LANR Quantum Electronic Device at MIT**, *J. Condensed Matter Nucl. Sci.* 13, (2014), p 516 www.iscmns.org/CMNS/JCMNS-Vol13.pdf

[3] M.R. Swartz, Hagelstein P.I., Demonstration of Energy Gain from a Preloaded ZrO2–PdD Nanostructured CF/LANR Quantum Electronic Device at MIT, J. Cond.Matter Nucl. Sci. 13, (2014), 516 www.iscmns.org/CMNS/JCMNS-Vol13.pdf

[4] M.R. Swartz, Verner, G. M., Tolleson, J., Wright, L., Goldbaum, R., Hagelstein, P. L., Amplification and restoration of energy gain using fractionated magnetic fields on Zr02-PdD nanostructured components, *J. Condensed Matter Nucl. Sci.* 15 (2015) 66. www.iscmns.org/CMNS/JCMNS-VoI15.pdf.

[5] M.R. Swartz, Incremental High Energy Emission from a ZrO2–PdD Nanostructured Quantum Electronic Component CF/LANR, J. Cond. Matter Nucl. Sci. 15, 2015, 92; www.iscmns.org/CMNS/JCMNS-Vol15.pdf
[6] M.R. Swartz, Verner, G., et al., Imaging of an Active NANOR®-type LANR Component using CR-39, J. Condensed Matter Nucl. Sci. 15, (2015), p 81; www.iscmns.org/CMNS/JCMNS-Vol15.pdf
[7] M.R. Swartz, P. Hagelstein, G. Verner, Impact of Electrical Avalanche Through a ZrO2-NiD Nanostructured Component on its Incremental Excess Power Gain", ICCF-19, JCMNS, 19, (2016)
[8] M.R. Swartz, "Detection of Phonon Gain from a NANOR®-type CF Component" (2016, in preparation and review)
[9] M.R. Swartz, G. Verner, "**Excess Heat from Low Electrical Conductivity Heavy Water Spiral-Wound Pd/D2O/Pt and Pd/D2O-PdCl2/Pt Devices**", *Condensed Matter Nuclear Science, Proc.ICCF-10*, World Scientific Publishing, ISBN 981-256-564-6, 29-44; 45-54 (2006).
[10] M.R. Swartz, **Excess Power Gain using High Impedance and Codepositional LANR Devices Monitored by Calorimetry, Heat Flow, and Paired Stirling Engines**, *Proc. ICCF14* 1, (2008), 123; ISBN: 978-0-578-06694-3, 123, (2010); www.iscmns.org/iccf14/ProcICCF14a.pdf
[11] M.R. Swartz, "**Survey of the Observed Excess Energy and Emissions In Lattice Assisted Nuclear Reactions**", *Journal of Scientific Exploration*, 23, 4, 419-436 (2009).
[12] J. Marwan, M. C. H. McKubre, F. L. Tanzella, P. L. Hagelstein, M. H. Miles, Edmund Storms, Y. Iwamura, P. A. Mosier-Boss and L. P. G. Forsley, "A new look at low-energy nuclear reaction (LENR) research: a response to Shanahan", J. Environ. Monit., (2010).
[13] M.R. Swartz, G. Verner, A. Frank, H. Fox "Importance of Non-dimensional Numbers and Optimal Operating Points in Cold Fusion", Journal of New Energy, 4, 2, 215-217 (1999).
[14] D. Cravens, "Factors Affecting Success Rate of Heat Generation in CF Cells", Proc. ICCF-4
[15] S. Szpak, P.A. Mosier-Boss, and F.E. Gordon, "Further Evidence of Nuclear Reactions in the Pd/D Lattice: Emission of Charged Particles," Naturwissenschaften, 94 (2007) 511-514.
[16] M.R. Swartz, "Impact of an Applied Magnetic Field on the Electrical Impedance of a LANR Device", Volume 4 JCMNS, Proc. March 2010, New Energy Technology Symposium held at the 239th American Chemical Society, San Francisco (2011).
[17] J. O'M. Bockris, R. Sundaresan, D. Letts and Z.S. Minevski, "Triggering and structural changes in Cold Fusion Electrodes", Proceedings ICCF4, Maui, Hawaii (1993).
[18] M.R. Swartz, "**P**husons in Nuclear Reactions in Solids**"**, *Fusion Technology*, 31, 228-236 (March 1997).
[19] D. L. R. Santos, P. Venezuela, R. B. Muniz, and A. T. Costa, "Spin pumping and interlayer exchange coupling through palladium", Phys. Rev. B 88, 054423 (2013)
[20] M.R. Swartz, "Scanning Vector Magnetometry of NANOR®-type Components" (2016, in preparation)
[21] J.M. Ok, Jo Y.J, Kim K, Shishidou T, Choi ES, Noh HJ, Oguchi T, Min BI, Kim JS. Quantum oscillations of the metallic triangular-lattice antiferromagnet PdCrO2. 3. Phys Rev Lett. 2013 Oct 25;111(17):176405 (2013).
[22] Shimizu Sunao, Kei S. Takahashi, Takafumi Hatano, Masashi Kawasaki, Yoshinori Tokura, and Yoshihiro Iwasa, Electrically Tunable Anomalous Hall Effect in Pt Thin Films, Phys. Rev. Lett. 111, 216803 (2013)
[23] Lattice configurations and magnetic oscillations in stacks of Josephson junctions, http://mti.msd.anl.gov/homepages/koshelev/projects/mag-osc.htm
[24] Brian Ahern on the late Arthur Manelas; personal communication (2015).
[25] Louis DeChiaro, L. Forsley, and P.A. Mosier-Boss, *Strained Layer Ferromagnetism in Transition Metals and its Impact Upon Low Energy Nuclear Reactions.* J. Cond. Matter Nucl. Sci., 2015.
[26] Shimizu, Sunao, Kei S. Takahashi, Takafumi Hatano, Masashi Kawasaki, Yoshinori Tokura, and Yoshihiro Iwasa, "Electrically Tunable Anomalous Hall Effect in Pt Thin Films", Phys. Rev. Lett. 111, 216803 (2013)
[27] Y. Sun, J. D. Burton and E. Y. Tsymbal, "Electrically driven magnetism on a Pd thin film", Phys. Rev. B 81, 064413, (2010)
[28] N. Takanol, T.Kai, K.Shiiki and F.Terasakil, "Effect of Copious Vacancies on Magnetism of Pd", Solid State Communications, Vol. 97, No. 2, pp. 153-156, (1996)
[29] M.R. Swartz, P.L.Hagelstein, Transient Vacancy Phase States in Palladium after High Dose-rate Electron Beam Irradiation, *J. Cond. Matter Nucl. Sci.* 14, (2014), 50
[30] J.R. Melcher, Continuum Electromechanics, The MIT Press (1981); ISBN-10: 026213165X; ISBN-13: 978-0262131650
[31] H.H. Woodson, Melcher.JR., "Electromechanical Dyanamics", Wiley &Sons (1968)
[32] A. R. von Hippel, Molecular science and molecular engineering", MIT Press (1959).